PNAS RESEARCH ARTICLE | APPLIED PHYSICAL SCIENCES OPEN ACCESS

Nanoscale dynamics of the cadherin–catenin complex bound to vinculin revealed by neutron spin echo spectroscopy

David J. E. Callaway[a,1], Iain D. Nicholl[b], Bright Shi[a,c], Gilbert Reyes[a,c], Bela Farago[d,1], and Zimei Bu[a,c,1]

Affiliations are included on p. 7.

Edited by David Weitz, Harvard University, Cambridge, MA; received April 28, 2024; accepted August 12, 2024

We report a neutron spin echo (NSE) study of the nanoscale dynamics of the cell–cell adhesion cadherin–catenin complex bound to vinculin. Our measurements and theoretical physics analyses of the NSE data reveal that the dynamics of full-length α-catenin, β-catenin, and vinculin residing in the cadherin–catenin–vinculin complex become activated, involving nanoscale motions in this complex. The cadherin–catenin complex is the central component of the cell–cell adherens junction (AJ) and is fundamental to embryogenesis, tissue wound healing, neuronal plasticity, cancer metastasis, and cardiovascular health and disease. A highly dynamic cadherin–catenin–vinculin complex provides the molecular dynamics basis for the flexibility and elasticity that are necessary for the AJs to function as force transducers. Our theoretical physics analysis provides a way to elucidate these driving nanoscale motions within the complex without requiring large-scale numerical simulations, providing insights not accessible by other techniques. We propose a three-way "motorman" entropic spring model for the dynamic cadherin–catenin–vinculin complex, which allows the complex to function as a flexible and elastic force transducer.

quasielastic neutron scattering | protein dynamics | nonequilibrium statistical mechanics | mechanotransduction | adherens junction

Significance

Proteins *move*! and do so on multiple time and length scales. Protein dynamics on nanoscales influences protein function but is at best difficult to observe and remains largely unexplored. We report a neutron spin echo (NSE) study revealing the activation of nanoscale dynamics in the cell–cell adhesion cadherin–catenin complex upon binding to vinculin. The complex acts as rigid *modules* connected by soft spring flexible linkers that exhibit overdamped nanoscale harmonic motions. The highly dynamic vinculin-bound cadherin–catenin complex provides the molecular flexibility that is necessary for the adherens junction to sense and transduce signals from the contractile transcellular cytoskeleton. We show that a simple analytical framework can identify the modes of internal motions in the complex without large-scale molecular dynamics simulations.

Neutron spin echo (NSE) is a quasielastic neutron scattering technique. NSE uses the fact that a neutron has a spin, and thus a magnetic moment, allowing one to employ the Larmor precession of neutrons in a magnetic field to measure the dynamics of matter at very high energy resolution (1). An advanced NSE spectrometer enables the measurements of dynamics on nanometer length scales and on 1 to 500 ns time scales (2). This makes NSE an ideal tool for studying protein dynamics (3–9). When combined with selective deuteration, theoretical physics, and complex reconstitution, NSE can uniquely measure the nanoscale dynamics of a multidomain protein in a multicomponent protein complex (4, 10). To analyze and interpret the NSE results, we have framed the problem in terms of mobility tensors, which provides a natural way to analyze the NSE data (3). In our theoretical framework, the translational mobility tensor defines the velocity response of a protein domain to a force applied to that domain or another domain, allowing the direct determination of nanoscale internal motion in a protein. Our theoretical framework is *analytical* and does not require large-scale molecular dynamics simulations. This theoretical analysis has been reviewed in detail elsewhere (11–13).

Adherens junctions (AJs) are specialized cell–cell adhesion complexes found in multicellular organisms (14). AJs bond between neighboring cells and provide mechanical strength to tissues. AJs also undergo dynamic remodeling during embryonic morphogenesis or wound healing so that migrating cells can continually break and remake cell–cell adhesive bonds to construct or repair the complex architectures of tissues (15). Disassembly of the AJs results in loss of cell polarity and contact inhibition, permitting cells to undergo epithelial-to-mesenchymal transition that is a necessary process during embryonic development (16). However, the epithelial-to-mesenchymal transition is often hijacked by metastatic cancers for uncontrolled invasion (17). Dysfunction of the AJs has also been implicated in vascular disease (18).

The core of the AJ is the cadherin–β-catenin–α-catenin (cadherin–catenin) complex (14, 19). Cadherin is a type I transmembrane protein that utilizes its extracellular domains to form a homophilic transcellular bond with another cadherin from a neighboring cell in a calcium-dependent manner (20). The intracellular domain of cadherin binds to β-catenin. β-catenin in turn interacts with the adapter protein α-catenin. α-catenin is an actin-binding protein that is thought to link the cadherin–β-catenin–α-catenin complex to the actin cytoskeleton. The linkage of the cadherin–catenin complex to the actin cytoskeleton is necessary for providing mechanical strength in cell–cell adhesions and for transmitting mechanical tensions between cells in quiescent tissues and during collective

Author contributions: D.J.E.C., I.D.N., B.F., and Z.B. designed research; D.J.E.C., B.S., G.R., B.F., and Z.B. performed research; D.J.E.C., B.F., and Z.B. contributed new reagents/analytic tools; D.J.E.C., B.F., and Z.B. analyzed data; I.D.N. and B.F. editing and reviewing the manuscript; and D.J.E.C. and Z.B. wrote the paper.

The authors declare no competing interest.

This article is a PNAS Direct Submission.

[1]To whom correspondence may be addressed. Email: dcallaway@ccny.cuny.edu, farago@ill.fr, or zbu@ccny.cuny.edu.

This article contains supporting information online at https://www.pnas.org/lookup/suppl/doi:10.1073/pnas.2408459121/-/DCSupplemental.

Published September 19, 2024.

cell migration (21, 22). Besides forming the cadherin–catenin complex, cadherin also associates with the cytosolic p120 catenin that stabilizes the cadherin at the membrane (23).

Studies have shown that the interaction of the cadherin–catenin complex with the actin microfilaments is force sensitive: Mechanical force or tension is required for the cadherin–catenin complex to bind effectively to the actin microfilament (F-actin) (24–26). This is in contrast to the α-catenin homodimer, which binds to the actin microfilament without requiring mechanical forces (27). In cells, mechanical forces are constitutively generated by the cytoskeletal actomyosin assemblies. The myosin motors produce pulling forces on the actin microfilaments, thereby causing tension within a microfilament as well as sliding movements between the microfilaments. The force-sensitive binding of the cadherin–catenin complex to the actomyosin assembly forms a transcellular mechanotransduction network that influences morphogenesis (28).

The core AJ cadherin–catenin complex associates with other intracellular proteins, which is necessary for the dynamic remodeling of the AJs (14, 29). In particular, vinculin is recruited to the AJs when cells are under recurrent high mechanical tension, such as during cell collective migration, or in epithelium, endothelium, and cardiomyocytes (30–34). Vinculin is an actin-binding protein and a mechanical force transducer that plays critical roles in both cell–cell and cell–matrix adhesion (35–37). The recruitment of vinculin to the AJ is essential for the proper development of heart and brain and for maintaining skin stem cell quiescence (31, 38–40). Upon recruiting to the AJ, vinculin collaborates with the cadherin–catenin complex to transduce mechanical forces between cadherin and the actin cytoskeleton (14, 31).

Biochemical and X-ray crystallographic studies showed that the D1 subdomain of vinculin head domain V_h binds to the vinculin-binding sequence (VBS) in the M1 subdomain of α-catenin, thereby unfurling the α-catenin M1 subdomain (Fig. 1 *A* and *B*), (41–43). However, it is not clear how vinculin modulates the structural dynamics of the full-length α-catenin and the cadherin–catenin complex. To gain molecular insight into how vinculin collaborates with the cadherin–catenin complex to transduce forces, we have determined the structure of the cadherin–catenin complex bound to full-length vinculin using small-angle neutron scattering (SANS) (44). This structural study revealed that the cadherin–catenin–vinculin complex is highly flexible.

To gain further insight into how vinculin influences the dynamics of the cadherin–catenin complex, here we report a NSE study of the nanoscale dynamics of the cadherin–catenin complex bound to full-length vinculin. We have biochemically reconstituted the cadherin–catenin–vinculin complex using selectively deuterated proteins, which allows NSE to measure the nanoscale dynamics of a hydrogenated component separately from an otherwise deuterated complex. Our theoretical physics analyses of the NSE data have revealed that the motion of the whole cadherin–catenin complex becomes activated when α-catenin as part of the cadherin–catenin complex binds to vinculin. Moreover, we found that vinculin is also dynamic, with the vinculin actin-binding domain (vinculin ABD) [also called the vinculin tail (Vt) domain] moving on the nanometer length scales and 1 to 500 ns timescales measured by NSE. As a result, the entire cadherin–catenin–vinculin complex is highly dynamic, involving nanoscale motions of this multiprotein multidomain complex. Such a highly dynamic cadherin–catenin–vinculin complex provides the molecular dynamics basis for the flexibility and elasticity of the vinculin-bound AJ. Molecular flexibility and elasticity are necessary characteristics of force transducers in cell–cell and cell–matrix adhesion, allowing them to respond to a variety changes of mechanical tension at cell–cell junctions (45) and the cell–matrix interface (36).

Results

We previously described the reconstitution of the complex of α-catenin–β-catenin–E-cadherin cytoplasmic tail (hereafter named as the ABE complex) (46) and the production of deuterated proteins (4, 9, 47–49). We note that the ABE complex is formed with high affinity, with the dissociation constant of β -catenin to E-cadherin cytoplasmic tail binding K_d = 19 nM and α-catenin binding to the β-catenin • E-cadherin (EcadCT) complex K_d = 120 nM (46).

Full-length vinculin adopts a head-to-tail autoinhibited conformation with the vinculin tail V_t domain folded back onto the vinculin head domain V_h, thus inhibiting V_h and V_t from binding to their respective targets. We showed that, by introducing mutations K944E, R945E, and K996E in the V_t domain to disrupt the salt bridges at the interface between V_h and V_t, which lock vinculin in the autoinhibited configuration, we generated a full-length open vinculin mutant that has high affinity for the α-catenin in the ABE complex (of dissociation constant K_d = 60 nM) (44). This open mutant of vinculin was named as VK3E. The full-length vinculin VK3E mutant binds to ABE at 1:1 stoichiometry ratio to form the VABE complex. This result is consistent with a previous biochemical and X-ray crystallography study (42) showing that no mechanical force is required for α-catenin to bind open vinculin. Details about generating the autoinhibition-disrupting mutants and reconstituting the VABE complex are described in our publication (44). We performed SANS on the selectively deuterated VABE complex. Our combined small-angle scattering and modeling analyses showed that the VABE complex contains multiple domains connected by flexible linkers (44), Fig. 1*A*. The steps to generate the structure of the VABE complex from combined small-angle scattering and Monte Carlo simulations analyses are outlined in *SI Appendix, Supplemental Materials 1*.

The following complexes were reconstituted for NSE measurements: 1) fully hydrogenated α-catenin.·β-catenin–E-cadherin cytoplasmic tail ($^{h}A^{h}B^{h}E$) complex bound to hydrogenated full-length vinculin autoinhibition-disrupting VK3E mutant to form the fully hydrogenated $^{h}V^{h}A^{h}B^{h}E$ complex; 2) deuterated VK3E bound to hydrogenated α-catenin, deuterated β-catenin, and deuterated E-cadherin cytoplasmic tail to form the selectively deuterated $^{d}V^{h}A^{d}B^{d}E$ complex, and 3) hydrogenated vinculin VK3E mutant bound to deuterated $^{d}A^{d}B^{d}E$ to form the selectively deuterated $^{h}V^{d}A^{d}B^{d}E$ complex.

In 100% D_2O buffer, NSE measures the dynamic intermediate function of a hydrogenated protein or protein complex, or the hydrogenated component in an otherwise deuterated protein complex (4). Fig. 2 shows the normalized intermediate functions I(q,t)/I(q,0) of the fully hydrogenated $^{h}V^{h}A^{h}B^{h}E$ complex (Fig. 2*A*), selectively deuterated $^{d}V^{h}A^{d}B^{d}E$ (Fig. 2*B*) and $^{h}V^{d}A^{d}B^{d}E$ complexes (Fig. 2*C*). All of our NSE experiments at Institut Laue-Langevin (ILL) IN15 have been performed at sufficiently low protein concentrations (4, 9, 10), so that the interparticle structure factor and interparticle hydrodynamic interference effects (8) are minimal in the q range measured by NSE. The measured I(q,t)/I(q,0) are thus the dynamic intermediate functions that represent the internal dynamics of a protein or a protein complex.

Fitting the initial slopes of $\ln[I(q,t)/I(q,0)]$ gives the decay rates (*SI Appendix*, Figs. S1 *B–D*, S2 *B–D*, and S3 *B–D*):

$$\Gamma(q) = \lim_{t\to 0} \frac{d \ln[\frac{I(q,t)}{I(q,0)}]}{dt}, \quad [1]$$

of the intermediate scattering functions. The effective diffusion coefficient as a function of q is then obtained as:

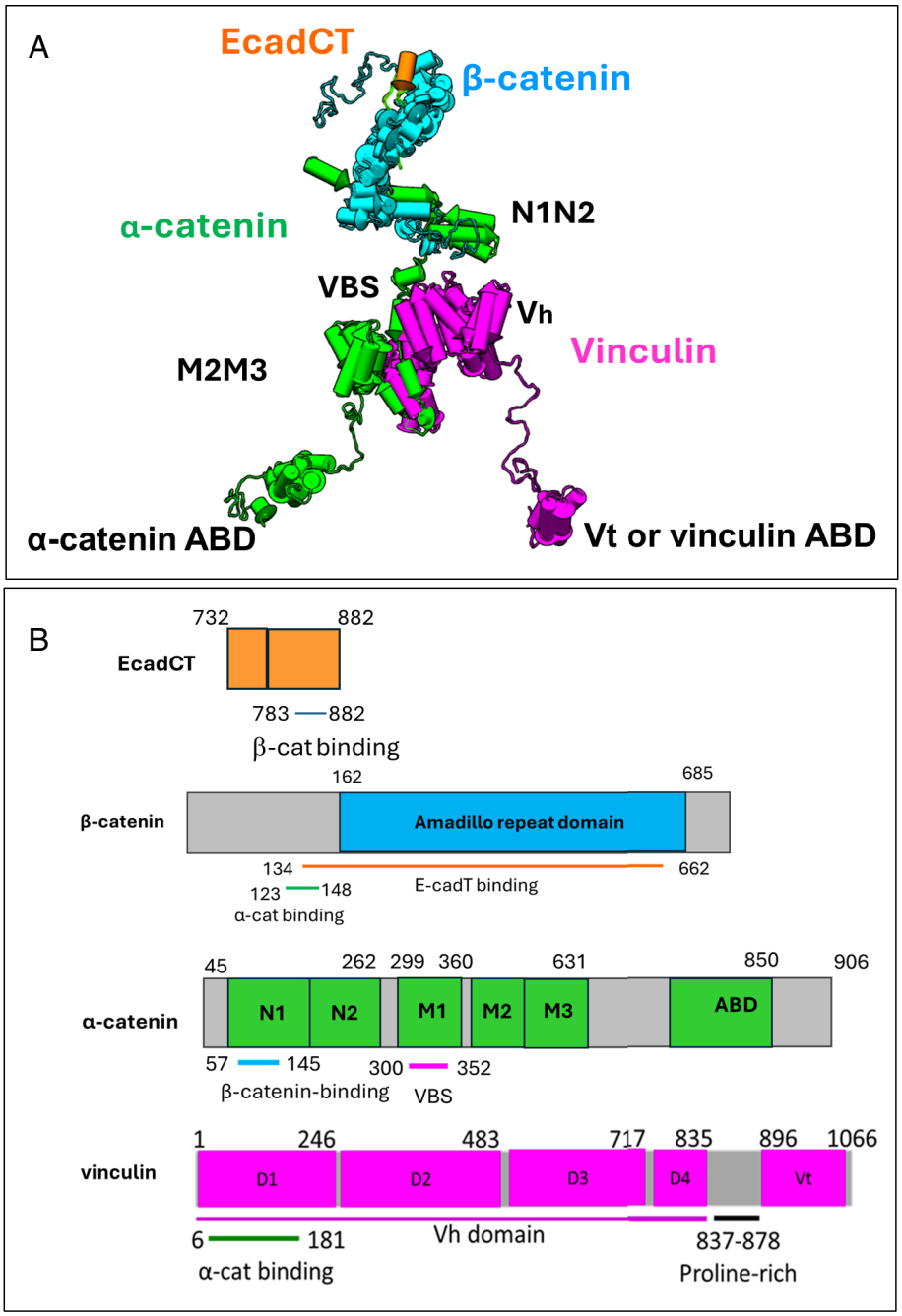

Fig. 1. Protein and domain organization of the VABE complex. (*A*) Structural model of VABE complex. The all-atomistic model shown represents an ensemble-averaged structure obtained from small-angle neutron and X-ray scattering as we reported previously (44). Also, see *SI Appendix, Supplemental Materials 1*. Outline of steps to construct VABE structure using small-angle X-ray and neutron scattering data. (*B*) Primary structure and domain arrangement of α-catenin, β-catenin, and vinculin.

$$D_{eff}(q) = \frac{\Gamma(q)}{q^2}. \quad [2]$$

$D_{eff}(q)$ of $^{h}V^{h}A^{h}B^{h}E$, $^{d}V^{h}A^{d}B^{d}E$, and $^{h}V^{d}A^{d}B^{d}E$ measured by NSE are shown in Fig. 2 *D–F*, respectively. The center-of-mass diffusion constant D_o of the VABE complex was measured by dynamic light scattering (DLS) using an inline DLS device installed at ILL IN15, *SI Appendix*, Fig. S4.

NSE Analysis. In solution, protein dynamics occurs in the low Reynolds number Brownian dynamics regime. Here, dynamics depends upon the size of the object but not its mass (50). The NSE results are thus best analyzed in terms of the mobility tensors H. We generalize the remarkable Akcasu–Gurol formula (51) to include rotational diffusion (3). The effective diffusion coefficient $D_{eff}(q)$ for a rigid body or for a body of multiple modules or domains is calculated as:

$$D_{eff}(q) = \frac{k_B T}{q^2} \frac{\sum_{jl} b_j b_l \left(q \cdot H_T^{jl} \cdot q + L_j \cdot H_R^{jl} \cdot L_l \right) e^{iq \cdot \left(r_j - r_l \right)}}{\sum_{jl} b_j b_l e^{iq \cdot \left(r_j - r_l \right)}}, \quad [3]$$

where $k_B T$ is the temperature factor and b_j is the scattering length of a subunit j (b_j is taken without loss of generality as 1 for the hydrogenated proteins and 0 for the deuterated proteins). $L_j = r_i \times q$ is the torque vector for each atom, H^T is the translational mobility tensor (defining the velocity response v to a given applied force F

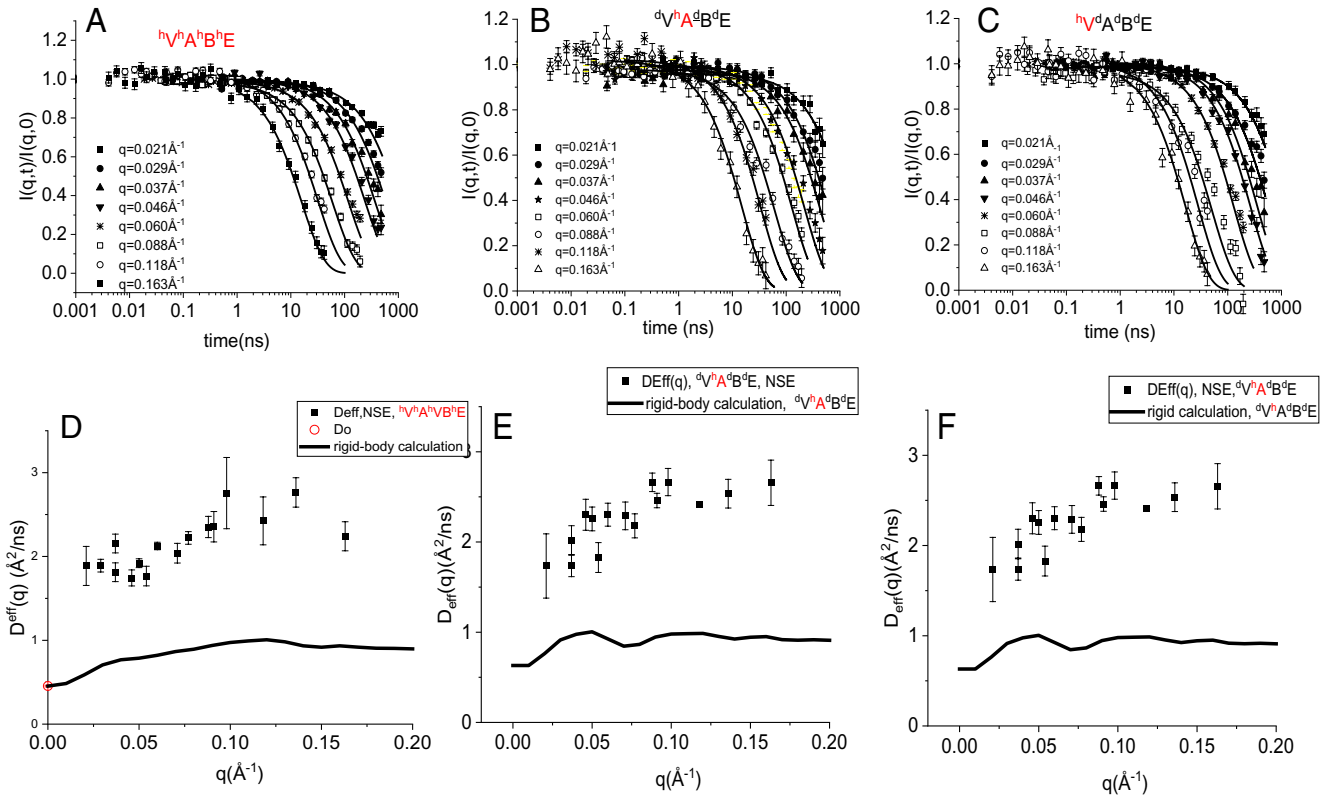

Fig. 2. NSE spectra and $D_{eff}(q)$ of VABE complexes. (*Upper*) NSE measured I(q,t) / I(q,0) for (*A*) fully hydrogenated $^{h}V^{h}A^{h}B^{h}E$, (*B*) selectively deuterated $^{d}V^{h}A^{d}B^{d}E$, and (*C*) $^{h}V^{d}A^{d}B^{d}E$ complexes. (*Lower*) $D_{eff}(q)$ of (*D*) ^{hVhAhBhE}, (*E*) $^{d}V^{h}A^{d}B^{d}E$, (*F*) $^{h}V^{d}A^{d}B^{d}E$. The full spectra and initial slope fittings are shown in *SI Appendix*, Figs. S1–S3.

by $v = H^{T}F$), and H^{R} is the rotational mobility tensor (defining the angular velocity response ω to a given applied torque τ by $\omega = H^{R}\tau$).

It is essential to note that the mobility tensors *define* internal molecular motion. For a rigid body, all pairs of atoms are included in the numerator in Eq. **3**. When a protein or protein complex (such as the VABE complex) is parsed into different separately moving modules or domains, only pairs of atoms both contained within a given module or domain are included in the numerator. The diffusion constant per atom is chosen uniformly for a given parsing for the *fully hydrogenated* complex so that $D_{eff}(q = 0)$ equals the experimentally measured diffusion constant D_0 of the complex. This value of the diffusion constant per atom is retained for the deuterated proteins. The mobility tensors are then calculated using a given hypothesized parsing of the complex into separately moving modules, the experimentally measured diffusion constant D_0, and the molecular structural coordinates of the complex. The overall strategy then is to propose a hypothetical parsing of the complex into modules, calculate (via Eq. **3**) the effective diffusion constant $D_{eff}(q)$ for each hypothetical parsing, and test the hypotheses by comparing the results for each parsing with the experimental NSE data. Further details can be found in our reviews (12, 13, 47, 52) and are summarized in *SI Appendix, Supplementary Materials 2*.

We first parsed the VABE complex into a single rigid body and then, progressively two, three, and four module models. The models are displayed in Figs. 3 and 4. In Fig. 3, we show the parsing into three modules, with each module being a protein that builds up the complex. Module 1 is the entire protein vinculin, module 2 is the entire protein β-catenin, and module 3 is the entire protein α-catenin. In Fig. 3*A*, the three modules move in unison—thus, the whole complex is taken as a rigid body. In Fig. 3 *B*–*D*, two modules move in unison, while the third moves separately, as indicated by the colors in the figures. In Fig. 3*E*, all of the three modules move independently but are connected by soft spring linkers. The resultant $D_{eff}(q)$ for each of the five models of the fully hydrogenated complex is shown in Fig. 3*F*. The model displayed in Fig. 3*E* with all three modules moving independently fits the experimental data best.

Our SANS studies (44) show that the ensemble-averaged structure of the VABE complex resembles a humanoid motorman with two flexible legs and a trunk mounted on a soft spring linker, Figs. 1*A* and 4. We next consider a parsing of the "motorman" VABE complex into four modules, as shown in Fig. 4, which are different from the 3-module parsing shown in Fig. 3:

Module 1 (hip of motorman), shown in blue in Fig. 4*D*, includes the V_h domain of vinculin, the VBS of α-catenin, and the M2M3 subdomains of α-catenin.

Module 2 (trunk of motorman), shown in cyan in Fig. 4*D*, includes β-catenin, EcadCT, the α-catenin N1N2 subdomains, and the linker between α-catenin N2 and α-catenin VBS.

Module 3 (one leg of motorman), shown in green in Fig. 4*D*, includes the linker between α-catenin M domain and α-catenin ABD, and the α-catenin ABD.

Module 4 (2nd leg of motorman) shown in magenta in Fig. 4*D* is the linker between V_h and V_t, and the vinculin ABD or V_t domain.

We performed calculations for the following models: 1) treating the complex as rigid, with modules 2, 3, and 4 moving in unison with module 1, which is the same rigid-body model shown in Fig. 3*A*; 2) two modules taken as moving in unison, with the other two modules moving independently, Fig. 4 *A*–*C*; and 3) all four modules moving independently, Fig. 4*D*. Fig. 4*E* displays the calculated $D_{eff}(q)$ for the fully hydrogenated complex for the rigid-body and all hypothetical models shown in Fig. 4 *A*–*D* and

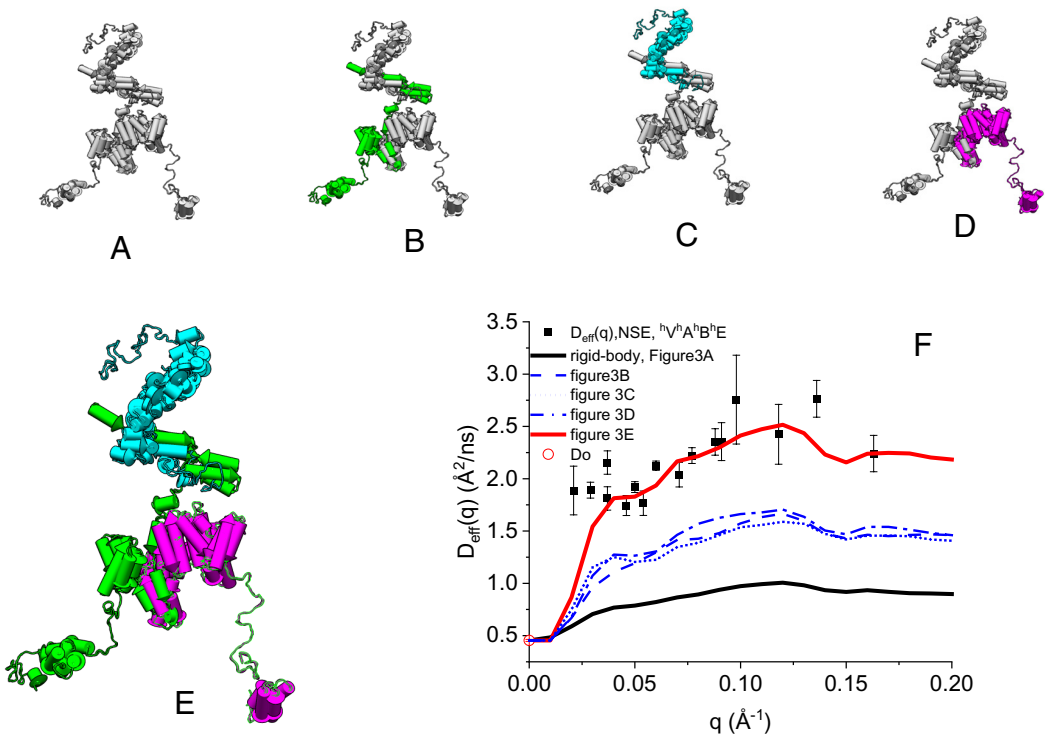

Fig. 3. Analysis of NSE result—the 3-module model of motion in VABE complex. (*A*) all proteins in VABE complex are rigid (all gray), (*B*) β-catenin and vinculin are rigid (gray), but α-catenin is dynamic with motions (green), (*C*) α-catenin and vinculin are rigid (gray), but β-catenin is dynamic (cyan), (*D*) α-catenin and β-catenin are rigid (gray) but vinculin is dynamic (magenta), (*E*) all proteins in VABE are dynamic, moving as independent modules, (*F*) comparing NSE D_{eff}(q) with those calculated from models (*A*–*E*).

shows that model D with all four modules moving independently fits the NSE data best. Our calculations thus show that the rigid body and two-module models are clearly excluded by the NSE data, However, the 3-module and the 4-module motorman models both fit the NSE data well. Additional calculations on the selectively deuterated complexes confirm that the 3-module and 4-module models both fit the experimental data, *SI Appendix*, Fig. S5. Thus, further subdivision is of limited utility.

Comparing the calculations with the NSE data suggests that the VABE complex is highly dynamic with activated motions in alpha-catenin, β-catenin, and in vinculin. Notably, the NSE measurements, interpreted by our calculations, reveal that upon recruiting vinculin to the cadherin–catenin complex, the motion of the entire α-catenin is activated. This is in stark contrast to the α-catenin homodimer, in which our previous NSE study showed that only the small disordered C-terminal tail attached to α-catenin ABD is moving, while the majority of α-catenin behaves as a rigid body (9). The activated dynamic motion of the whole α-catenin as part of the VABE complex is also strikingly different from that of α-catenin as part of the ABE complex, in which our NSE study revealed that the motion of the larger α-catenin ABD is activated (10).

Discussion

The NSE experiments and analyses show that, in the VABE complex, at least three modules are moving on 1 to 500 ns time scales and on nanometer length scales. This is remarkably different from the dynamics of the α-catenin homodimer or that of the α-catenin as part of the cadherin–catenin complex. Our series of NSE studies thus demonstrate the increasingly enhanced nanoscale domain motions in α-catenin homodimer, when α-catenin is incorporated into the cadherin–catenin complex, and when α-catenin recruits vinculin to form the cadherin–catenin–vinculin complex. Notably, the change in nanoscale dynamics of the cadherin–catenin complex and the VABE complex, as revealed by NSE, is a spatial-temporal dynamic regime that is not approachable by any contemporary structural biology or single-molecule measurements. We also stress that our theoretical analysis is *analytical* throughout and does not require large-scale molecular dynamics simulations, which are based on largely ad hoc empirical force fields.

The Cadherin–Catenin–vinculin Complex Is a Three-Way Motorman Entropic Spring That Is Flexible and Elastic. Alpha-catenin and vinculin are force transducers between the cell adhesion sites and the actin cytoskeleton (24, 53). In-cell single-molecule fluorescence resonance energy transfer (smFRET) studies have demonstrated that α-catenin and vinculin undergo cycles of rapid and repeated conformational changes in response to altered tensions at cell–cell junctions (45), and at cell–matrix focal adhesion sites (36), respectively. Furthermore, a study by Shoyer et al. has revealed that the "loadable" or open conformation of vinculin is recruited to cell–cell junctions during collective cell migration (54). Perturbing the ability of vinculin to change its conformation, by phosphorylation mimetics at the vinculin V_t domain, alters the speed and long-range coordination of collective cell migration. In one of our previous studies using NSE (7), we noticed a related effect, in that phosphorylation mimetics changed the nanoscale dynamics of an adapter protein NHERF1 (but not its structure or conformation), which altered NHERF1 binding kinetics to Ezrin (7).

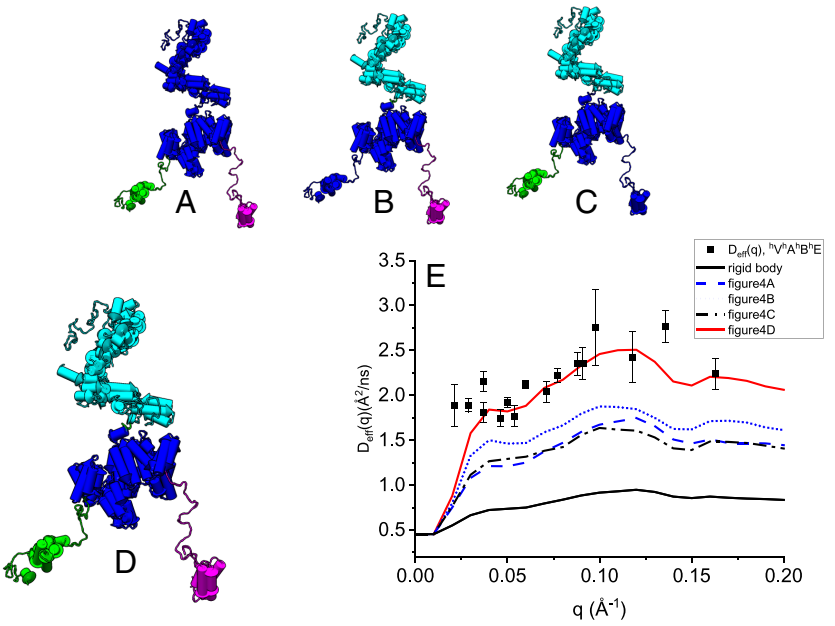

Fig. 4. The 4-module model of motion in VABE complex. (*A*) Motorman trunk and hip are rigid (blue), but two legs (green and magenta) are dynamic. (*B*) motorman hip and the α-catenin leg are rigid (blue), but the trunk (cyan) and the vinculin leg (magenta) are dynamic. (*C*) Motorman hip and the vinculin leg are rigid (blue), but the trunk (cyan) and the α-catenin leg (green) are dynamic. (*D*) All four modules of motorman, trunk (cyan), hip (blue), and two legs (green and magenta) are dynamic. (*E*) Comparing NSE $D_{eff}(q)$ with those calculated from models (*A*–*D*).

Collectively these smFRET studies suggest that α-catenin and vinculin are flexible and elastic as force transducers—so that these force transducers are entropic springs. Notably, the smFRET studies revealed the conformational changes in the linker region preceding the actin-binding modules of α-catenin and vinculin (36, 45), which correspond to the leg modules of the motorman shown in Fig. 4. The conformational changes measured by the above smFRET are on longer time scales than the nanoscale dynamics measured by our NSE experiments. Nevertheless, nanoscale dynamics inspires the longer temporal conformational dynamics observed in single-molecule experiments (55).

Vinculin is recruited to the AJ when cells are under increased mechanical tension. Our NSE analysis reveals that the vinculin-bound AJ complex is more dynamic than the core AJ cadherin–catenin complex alone. As a result, the vinculin-bound AJ is more flexible and more elastic to meet the demand of recurrent and enhanced cell–cell junction tensions. Flexibility and elasticity are important physical traits of cellular force transducers (56). Here, our dynamics analysis of the VABE complex details the modes of activated nanoscale motions in these force transducers as they combine to form the cadherin–catenin–vinculin complex. The activated nanoscale protein motions in the motorman-like VABE complex provide the molecular dynamics basis for the cadherin–catenin–vinculin complex to be flexible and elastic (57, 58), so as to respond to and to transduce a multitude of cell–cell junction forces, such as during collective cell migration.

Studies have demonstrated that α-catenin as part of the cadherin–catenin complex does not bind to the F-actin microfilament under zero force (26) and that mechanical tension is required to enable α-catenin as part of the cadherin–catenin complex to bind the F-actin microfilament (25). We previously showed that activated nanoscale domain motion in α-catenin ABD (46) as part of the ABE complex is correlated with increased conformational entropy in the ABE complex (10). We proposed that this increased conformational entropy serves as a negative allosteric regulatory mechanism, which impedes the α-catenin ABD as part of the cadherin–catenin complex from binding to F-actin under zero force. Mechanical tension can reduce the conformational entropy in α-catenin as part of the cadherin–catenin complex (25), so that the cadherin–catenin complex can bind to an F-actin microfilament under mechanical tension.

Upon recruiting vinculin to the cadherin–catenin complex, here, we find that α-catenin becomes even more dynamic, with activated dynamic motions in the whole α-catenin protein. This finding corroborates our previous biochemical and structural study that α-catenin as part of the VABE complex does not bind actin microfilaments under zero force, but the VABE complexes employ vinculin as the major actin-binding mode (44). The elevated nanoscale dynamics in the entire α-catenin as part of the VABE complex may contribute additional conformational entropy that further negatively regulates (or impedes) α-catenin from binding to actin microfilament, thus requiring an even larger magnitude of force for α-catenin to bind actin microfilament. Nevertheless, once bound to F-actin at high tension, the flexible α-catenin and vinculin in the VABE complex may have prolonged lifetimes bound to the cytoskeletal actin, which can then endure high tension before dissociating from the cytoskeletal actin microfilament. Thus, in the vinculin-bound AJ complex, the enhanced dynamics of the α-catenin is likely tuned for sensing and transducing higher magnitude forces.

Our NSE analysis shows that in the VABE complex, the activated nanoscale dynamics span the motorman trunk, hip, and the two legs, Fig. 4. Recent studies found that vinculin is essential for sustaining a "normal level of endogenous forces" at the AJs (59). The motorman model of the VABE complex provides a structural dynamics explanation for this alternative β-catenin-vinculin interaction: Under low force, the cadherin–catenin–vinculin complex employs the vinculin motorman leg to bind cytoskeletal actin, without the α-catenin leg participating in actin binding. The motorman trunk module that is composed of β-catenin and EcadCT transmits the force from the vinculin leg to the extracellular domain

of cadherin. At high tension, both the motorman vinculin and α-catenin legs interact with cytoskeletal actin, and the motorman trunk module (β-catenin and EcadCT) integrates and transmits the forces from both legs to the extracellular domain of cadherin.

Studies find that β-catenin binds to vinculin directly (60). Our structural analysis indicates that in the VABE complex, a fraction of β-catenin has extended conformation with the N-terminal tail in contact to the V_h domain of vinculin (44). Such interaction between V_h and β-catenin N-terminal tail may contribute additively to the motion of the motorman trunk module

Vinculin, β-catenin, and α-catenin are critical adapter proteins that couple the AJs to the cytoskeletal actin of neighboring cells. The nanoscale dynamics of α-catenin, vinculin, and β-catenin in the cadherin–catenin–vinculin complex, as revealed in the NSE studies, inspires the longer timescale motions that are observed by smFRET (36, 45, 54). The control of protein flexibility and elasticity underscores the importance of nanoscale dynamics of the AJ complex in sensing, bearing, and transmitting mechanical tensions of multiple magnitudes from the cellular cytoskeleton to the transcellular cell–cell adhesion sites. Our motorman modular model of nanoscale dynamics of the VABE complex provides the structural dynamics mechanism to explain the force transmission functions of the AJ as vinculin is recruited to the AJ.

Materials and Methods

Protein Purification and Protein Complex Reconstitution. The bacterial expression and fast protein liquid chromatography purification of full-length human αE-catenin, human β-catenin, the cytoplasmic domain of human EcadCT (residues 731 to 882), and the full-length human vinculin autoinhibition-disruption mutant VK3E have been described previously (44, 46). Deuterated αE-catenin, β-catenin, VK3E, and EcadCT were grown in 85% D_2O (vol/vol) M9 medium following the protocols described in refs. 47, and 48. The purification of deuterated proteins was the same as that of the hydrogenated proteins. Reconstitution of the hydrogenated $^{h}A^{h}B^{h}E$ and selectively deuterated $^{h}A^{d}B^{d}E$ complexes followed the same protocol as we described previously (46). Reconstitution of the fully hydrogenated $^{h}V^{h}A^{h}B^{h}E$ and selectively deuterated $^{h}V^{d}A^{d}B^{d}E$ and $^{d}V^{h}A^{d}B^{d}E$ complex was described in a previous publication (44).

Before the NSE experiments, a phosphate-buffered saline (PBS) tablet (ThermoFisher, Waltham, MA) for making 500 mL 1× PBS buffer was soaked in 2 mL 99.9% D_2O and vacuum dried at 80 °C for five cycles to exchange the H in the tablet to D. The D-exchanged PBS tablet was added to 500 mL 99.9% D_2O to make the D_2O PBS buffer. The protein complexes were then exchanged into the D_2O PBS buffer using a Vivaspin 20 centrifugal concentrator of 10 kDa molecular weight cut-off (Sartorius Stedim North America Inc, Bohemia, NY). The NSE measured protein concentrations were 10.86 mg/mL for the $^{h}V^{h}A^{h}B^{h}E$ complex, 13.1 mg/mL for the $^{d}V^{h}A^{d}B^{d}E$ complex, and 12.4 mg/mL for the $^{h}V^{d}A^{d}B^{d}E$ complex.

NSE Measurements. The NSE experiments were performed with the upgraded high-resolution IN15 instrument at the ILL (2). We used three different wavelengths: 6, 10, and 13.5 Å covering 0.5 to 42, 0.2 to 194, and 0.4 to 477-ns time intervals. The covered Fourier time scales with the third power of the wavelength, but the incoming flux also drops roughly with the fourth power. The choice of the wavelength was made by optimizing the compromise between the resolution need and the incoming neutron flux. The beam monochromatization in each case was 15% full width at half-maximum as given by the neutron velocity selector. The samples were filled in quartz cells with 2-mm sample thickness, and the temperature was controlled at 10.0 ± 0.1 °C. Instrumental resolution was measured from the standard Grafoil (GrafTech, Lakewood, OH), which gives a strong, elastic, coherent small-angle scattering. The background was measured on the PBS D_2O buffer, and the sample spectra were corrected using the relative transmissions following the standard procedures. The sample environment box is equipped with a home-designed DLS apparatus where optical monomodal fibers bring in the laser light and collect scattered light at 90° scattering angle. All optics is placed below the neutron beam to avoid radiation damage. The correlator is a FLEX02-01D multitau digital correlator by Correlator.com LTD. During the NSE measurement, the DLS is run repeatedly to monitor for potential sample aging. In our case, both the scattered light intensity and the relaxation rate were constant within accuracy.

Data Management-ILL Neutrons for Society. 10.5291/ILL-DATA.8-04-942.

Data, Materials, and Software Availability. NSE spectra data have been deposited in Data Management-ILL Neutrons for Society: 10.5291/ILL-DATA.8-04-942 (61).

ACKNOWLEDGMENTS. This research was funded by NSF Grant MCB–2202202. B.S. and G.R. were supported by G-RISE Ph.D. traineeships from the NIH (Grant #T32GM136499).

Author affiliations: [a]Department of Chemistry and Biochemistry, City College of New York, City University of New York, New York, NY 10031; [b]Department of Biomedical Science and Physiology, Faculty of Science and Engineering, University of Wolverhampton, Wolverhampton WV1 1LY, United Kingdom; [c]Ph.D. Programs in Chemistry and Biochemistry, City University of New York Graduate Center, New York, NY 10016; and [d]High-Resolution Spectroscopy Group, Institut Laue-Langevin, F-38042 Grenoble Cedex 9, France

1. F. Mezei, "The principles of neutron spin echo" in *Neutron Spin Echo: Proceedings of a Laue-Langevin Institut Workshop*, F. Mezei, Eds. (Springer, Heidelberg, 1980), pp. 1–26.
2. B. Farago *et al.*, The IN15 upgrade. *Neutron News* **26**, 15 (2015).
3. Z. Bu, R. Biehl, M. Monkenbusch, D. Richter, D. J. Callaway, Coupled protein domain motion in Taq polymerase revealed by neutron spin-echo spectroscopy. *Proc. Natl. Acad. Sci. U.S.A.* **102**, 17646–17651 (2005).
4. B. Farago, J. Li, G. Cornilescu, D. J. Callaway, Z. Bu, Activation of nanoscale allosteric protein domain motion revealed by neutron spin echo spectroscopy. *Biophys. J.* **99**, 3473–3482 (2010).
5. J. Lal, P. Fouquet, M. Maccarini, L. Makowski, Neutron spin-echo studies of hemoglobin and myoglobin: Multiscale internal dynamics. *J. Mol. Biol.* **397**, 423–435 (2010).
6. A. M. Stadler *et al.*, Internal nanosecond dynamics in the intrinsically disordered myelin basic protein. *J. Am. Chem. Soc.* **136**, 6987–6994 (2014).
7. D. J. Callaway *et al.*, Controllable activation of nanoscale dynamics in a disordered protein alters binding kinetics. *J. Mol. Biol.* **429**, 987–998 (2017).
8. Y. Liu, Intermediate scattering function for macromolecules in solutions probed by neutron spin echo. *Phys. Rev. E* **95**, 020501 (2017).
9. I. D. Nicholl *et al.*, alpha-Catenin structure and nanoscale dynamics in solution and in complex with F-Actin. *Biophys. J.* **115**, 642–654 (2018).
10. B. Farago *et al.*, Activated nanoscale actin-binding domain motion in the catenin-cadherin complex revealed by neutron spin echo spectroscopy. *Proc. Natl. Acad. Sci. U.S.A.* **118**, e2025012118 (2021).
11. Z. Bu, D. J. Callaway, Proteins MOVE! Protein dynamics and long-range allostery in cell signaling. *Adv. Protein Chem. Struct. Biol.* **83**, 163–221 (2011).
12. D. J. Callaway, B. Farago, Z. Bu, Nanoscale protein dynamics: A new frontier for neutron spin echo spectroscopy. *Eur. Phys. J. E Soft Matter* **36**, 9891 (2013).
13. D. J. Callaway, Z. Bu, Visualizing the nanoscale: Protein internal dynamics and neutron spin echo spectroscopy. *Curr. Opin. Struct. Biol.* **42**, 1–5 (2017).
14. M. Takeichi, Dynamic contacts: Rearranging adherens junctions to drive epithelial remodelling. *Nat. Rev. Mol. Cell Biol.* **15**, 397–410 (2014).
15. B. M. Gumbiner, Cell adhesion: The molecular basis of tissue architecture and morphogenesis. *Cell* **84**, 345–357 (1996).
16. R. Kalluri, EMT: When epithelial cells decide to become mesenchymal-like cells. *J. Clin. Invest.* **119**, 1417–1419 (2009).
17. D. Hanahan, R. A. Weinberg, Hallmarks of cancer: The next generation. *Cell* **144**, 646–674 (2011).
18. M. G. Lampugnani, E. Dejana, C. Giampietro, Vascular endothelial (VE)-cadherin, endothelial adherens junctions, and vascular disease. *Cold Spring Harb. Perspect. Biol.* **10**, a029322 (2018).
19. L. Shapiro, W. I. Weis, Structure and biochemistry of cadherins and catenins. *Cold Spring Harb. Perspect. Biol.* **1**, a003053 (2009).
20. J. Brasch, O. J. Harrison, B. Honig, L. Shapiro, Thinking outside the cell: How cadherins drive adhesion. *Trends Cell Biol.* **22**, 299–310 (2012).
21. R. Mayor, S. Etienne-Manneville, The front and rear of collective cell migration. *Nat. Rev. Mol. Cell Biol.* **17**, 97–109 (2016).
22. D. Cai *et al.*, Mechanical feedback through E-cadherin promotes direction sensing during collective cell migration. *Cell* **157**, 1146–1159 (2014).
23. M. A. Davis, R. C. Ireton, A. B. Reynolds, A core function for p120-catenin in cadherin turnover. *J. Cell Biol.* **163**, 525–534 (2003).
24. S. Yonemura, Y. Wada, T. Watanabe, A. Nagafuchi, M. Shibata, alpha-Catenin as a tension transducer that induces adherens junction development. *Nat. Cell Biol.* **12**, 533–542 (2010).
25. C. D. Buckley *et al.*, Cell adhesion. The minimal cadherin-catenin complex binds to actin filaments under force. *Science* **346**, 1254211 (2014).
26. S. Yamada, S. Pokutta, F. Drees, W. I. Weis, W. J. Nelson, Deconstructing the cadherin-catenin-actin complex. *Cell* **123**, 889–901 (2005).

27. D. L. Rimm, E. R. Koslov, P. Kebriaei, C. D. Cianci, J. S. Morrow, Alpha 1 (E)-catenin is an actin-binding and-bundling protein mediating the attachment of F-actin to the membrane adhesion complex. *Proc. Natl. Acad. Sci. U.S.A.* **92**, 8813–8817 (1995).
28. N. C. Heer, A. C. Martin, Tension, contraction and tissue morphogenesis. *Development* **144**, 4249–4260 (2017).
29. O. Campàs, I. Noordstra, A. S. Yap, Adherens junctions as molecular regulators of emergent tissue mechanics. *Nat. Rev. Mol. Cell Biol.* **25**, 252–269 (2024).
30. J. R. Carvalho *et al.*, Non-canonical Wnt signaling regulates junctional mechanocoupling during angiogenic collective cell migration. *Elife* **8**, e45853 (2019).
31. R. Biswas *et al.*, Mechanical instability of adherens junctions overrides intrinsic quiescence of hair follicle stem cells. *Dev. Cell* **56**, 761–780.e7 (2021).
32. C. D. Merkel, Y. Li, Q. Raza, D. B. Stolz, A. V. Kwiatkowski, Vinculin anchors contractile actin to the cardiomyocyte adherens junction. *Mol. Biol. Cell* **30**, 2639–2650 (2019).
33. S. Huveneers *et al.*, Vinculin associates with endothelial VE-cadherin junctions to control force-dependent remodeling. *J. Cell Biol.* **196**, 641–652 (2012).
34. F. Twiss *et al.*, Vinculin-dependent Cadherin mechanosensing regulates efficient epithelial barrier formation. *Biol. Open* **1**, 1128–1140 (2012).
35. J. L. Bays, K. A. DeMali, Vinculin in cell-cell and cell-matrix adhesions. *Cell Mol. Life Sci.* **74**, 2999–3009 (2017).
36. C. Grashoff *et al.*, Measuring mechanical tension across vinculin reveals regulation of focal adhesion dynamics. *Nature* **466**, 263–266 (2010).
37. P. M. Thompson, C. E. Tolbert, S. L. Campbell, Vinculin and metavinculin: Oligomerization and interactions with F-actin. *FEBS Lett.* **587**, 1220–1229 (2013).
38. A. E. Zemljic-Harpf *et al.*, Cardiac-myocyte-specific excision of the vinculin gene disrupts cellular junctions, causing sudden death or dilated cardiomyopathy. *Mol. Cell Biol.* **27**, 7522–7537 (2007).
39. I. Shiraishi *et al.*, Vinculin is an essential component for normal myofibrillar arrangement in fetal mouse cardiac myocytes. *J. Mol. Cell Cardiol.* **29**, 2041–2052 (1997).
40. W. Xu, H. Baribault, E. D. Adamson, Vinculin knockout results in heart and brain defects during embryonic development. *Development* **125**, 327–337 (1998).
41. H. J. Choi *et al.*, alphaE-catenin is an autoinhibited molecule that coactivates vinculin. *Proc. Natl. Acad. Sci. U.S.A.* **109**, 8576–8581 (2012).
42. E. S. Rangarajan, T. Izard, The cytoskeletal protein alpha-catenin unfurls upon binding to vinculin. *J. Biol. Chem.* **287**, 18492–18499 (2012).
43. Y. Hirano, Y. Amano, S. Yonemura, T. Hakoshima, The force-sensing device region of alpha-catenin is an intrinsically disordered segment in the absence of intramolecular stabilization of the autoinhibitory form. *Genes Cells* **23**, 370–385 (2018).
44. B. Shi *et al.*, An ensemble of cadherin-catenin-vinculin complex employs vinculin as the major F-actin binding mode. *Biophys. J.* **122**, 2456–2474 (2023).
45. T. J. Kim *et al.*, Dynamic visualization of α-catenin reveals rapid, reversible conformation switching between tension states. *Curr. Biol.* **25**, 218–224 (2015).
46. M. Bush *et al.*, An ensemble of flexible conformations underlies mechanotransduction by the cadherin-catenin adhesion complex. *Proc. Natl. Acad. Sci. U.S.A.* **116**, 21545–21555 (2019).
47. D. J. Callaway, Z. Bu, Essential strategies for revealing nanoscale protein dynamics by neutron spin echo spectroscopy. *Methods Enzymol.* **566**, 253–270 (2016).
48. X. Chen *et al.*, Phosphatidylinositol 4,5-bisphosphate clusters the cell adhesion molecule CD44 and assembles a specific CD44-Ezrin heterocomplex, as revealed by small angle neutron scattering. *J. Biol. Chem.* **290**, 6639–6652 (2015).
49. S. Bhattacharya *et al.*, Ligand-induced dynamic changes in extended PDZ domains from NHERF1. *J. Mol. Biol.* **425**, 2509–2528 (2013), 10.1016/j.jmb.2013.04.001.
50. J. Howard, *Mechanics of Motor Proteins and the Cytoskeleton* (Sinauer Associates, Sunderland, MA, 2001).
51. Z. Akcasu, H. Gurol, Quasi-elastic scattering by dilute polymer-solutions. *J. Polymer Sci. B Polymer Phys.* **14**, 1–10 (1976).
52. D. J. Callaway, Z. Bu, Nanoscale protein domain motion and long-range allostery in signaling proteins–A view from neutron spin echo sprectroscopy. *Biophys. Rev.* **7**, 165–174 (2015).
53. B. D. Hoffman, C. Grashoff, M. A. Schwartz, Dynamic molecular processes mediate cellular mechanotransduction. *Nature* **475**, 316–323 (2011).
54. T. C. Shoyer *et al.*, Coupling during collective cell migration is controlled by a vinculin mechanochemical switch. *Proc. Natl. Acad. Sci. U.S.A.* **120**, e2316456120 (2023).
55. W. Min *et al.*, Fluctuating enzymes: Lessons from single-molecule studies. *Acc. Chem. Res.* **38**, 923–931 (2005).
56. P. A. Janmey, D. A. Weitz, Dealing with mechanics: Mechanisms of force transduction in cells. *Trends Biochem. Sci.* **29**, 364–370 (2004).
57. P. De Gennes, Dynamics of entangled polymer solutions. I. The Rouse model. *Macromolecules* **9**, 587–593 (1976).
58. D. W. Urry, Entropic elastic processes in protein mechanisms. I. Elastic structure due to an inverse temperature transition and elasticity due to internal chain dynamics. *J. Protein Chem.* **7**, 1–34 (1988).
59. M. Mezher *et al.*, Vinculin is essential for sustaining normal levels of endogenous forces at cell-cell contacts. *Biophys. J.* **122**, 4518–4527 (2023).
60. X. Peng, L. E. Cuff, C. D. Lawton, K. A. DeMali, Vinculin regulates cell-surface E-cadherin expression by binding to beta-catenin. *J. Cell Sci.* **123**, 567–577 (2010).
61. B. Farago, Z. Bu, D. Callaway, I. Nicholl, Neutron Spin Echo Spectroscopy Study of the Dynamics of Cadherin-Catenin and Vinculin Complex. Institut Laue-Langevin (ILL). doi: https://doi.org/10.5291/ILL-DATA.8-04-942. Deposited 09 October 2023.